Selective Droplet Partitioning Using Single Layer Microfluidic Valves

Mohammad Reza Raveshi[a], Sagar N. Agnihotri[b], Muhsincan Sesen[a], Rajneesh Bhardwaj[c], Adrian Neild[*a]

[a] Department of Mechanical and Aerospace Engineering, Monash University, Melbourne, VIC 3800, Australia

[b] IITB-Monash research academy, IIT Bombay, Mumbai 400076, India

[c] Department of Mechanical Engineering, Indian Institute of Technology Bombay, Mumbai 400076, India.

[*]Corresponding author: adrian.neild@monash.edu (A.N.).

Abstract

Droplet microfluidics, with its small scale isolated samples, offers huge potential in the further miniaturisation of high throughput screening. The challenge is to deliver multiple samples in a manner such that reactions can be performed in numerous permutations. The present study investigates the use of single layer valves to subdivide individual droplets selectively. This partitioning of large droplets, allows the main sample volume to navigate around the chip, with smaller daughter droplets being removed at desired locations. As such, the mother droplet is no longer an isolated sample akin to an on-chip test tube, but rather a mobile sample delivery system akin to an on-chip pipette. The partitioning takes place at the entrance to a bypass loop of the main channel. Under normal operating conditions the droplet passes the entrance intact, however, when a valve located at the entrance to the bypass loop is actuated the geometry changes causes the droplet to split. We analyse this transition in behaviour for a range of oil and water inlet, and valve actuation pressures, showing that the valve can be actuated such that the next droplet to pass the bypass loop will be split, but subsequent droplets will not be.

1 Introduction

Droplet microfluidics are enclosed systems in which two immiscible phases are used, such that samples and reagents can be encapsulated in picolitre droplets within a continuous buffer where evaporation does not occur.[1] This partitioning of samples into isolated droplets, the lab-on-a-chip equivalent of a micro well plate, has been widely used for single cell analysis. Single cells can be captured and analysed in such microenvironments, allowing information to be gathered at the individual cell level across a whole population of cells. Other applications include nanoparticle production[2-4], creating micro structures for drug delivery vessels[5-7], and conducting high throughput screening[1,8]. The latter, would allow a new platform for conducting the type of combinatorial library reactions currently performed using microtiter plates. Here, banks of reagents are reacted with each other in numerous permutations, however, the plates cannot undergo further miniaturisation due to issues with pipette dispensing accuracy and evaporation.[9,10] Two phase droplet microfluidics provides an evaporation free environment so picolitres can be handled.[1] However, there are challenges around dispensing, or more specifically, the delivery of small sample volumes such that different chemicals can be reacted together in the desired combinations.[11]

The standard, passive tools for droplet microfluidics, such as droplet generation at channel junctions cause the same behaviour to occur repeatedly, for example, the partition of a sample flow into multiple droplets when merged with an immiscible buffer flow at a T-junction.[12] However, for the selective combination of multiple samples in different permutations, the challenge is to direct different samples to different locations at will so that an ordered matrix of droplets can be formed. Whilst there have been

considerable successes in this direction[8,13-16], there is still a need to develop improved methods to actively interact with single fluid samples to create[12,17-21], merge[3,22-35], trap[25,26,36] or divide[37,38] a droplet when desired.

The introduction of different samples onto a chip in relatively large volumes has been achieved by mechanical movement of the inlet connected to the channel between sample reservoirs[16]. The ability to halve or divide these plugs into daughter droplets would allow the controlled delivery of each sample into certain locations around a fluidic network. The ability to selectively subdivide becomes analogous to pipetting and dispensing from a well plate to another.[37] When combined with droplet merging mechanism, permutations of reactions can be performed from a library of samples.

A symmetric breaking-up of droplets, i.e. into two equal volumes, is desirable when splitting is used to increase the production rate of droplets, maximize the capacity of the device, or produce one set of equal size droplet for a control experiment.[39-43] However, when a controllable volume or concentration of chemicals inside the droplet is required in pharmaceutical or chemical industries, an asymmetric breaking up of droplets is required.[44-46] Methods for performing droplet splitting can be categorized into passive, active and combined methods.

Passive manipulation techniques utilize interactive effects between dispersed phase, continuous phase and channel structures without using any external fields. Methods include using a narrow orifice in a flow focusing junction which can cause the splitting of a plug into much smaller droplets,[47] the addition of a mid-channel obstacle[48] or bifurcating the channel.[48-50] as such, it can be seen that passive droplet splitting techniques need to simply be designed into the geometry of the chip, however, they act equally on all droplets without the possibility of selectivity.

A degree of control can be gained by the addition of active mechanisms to these passive geometric features. For example by adding an electrical field at a simple bifurcating junction can alter the relative size of the daughter droplets created.[51] Other methods include the use of electrostatic potential wells, a laser[52-54] or micro-heaters.[55,56] Whilst these methods improve the controllability of daughter droplet size there are some potential issues with biocompatibility. Other methods have used Electrowetting-on-Dielectric (EWOD) and Dielectrowetting to control the splitting in a bifurcation through contact line control[57,58] and surface acoustic waves (SAW) which have been used to apply forces on the interface between the immiscible fluids to split and steer droplets.[38,59] Finally, the droplet as pipette concept has been shown by altering the flow field locally at a bifurcation using acoustic streaming created by surface acoustic waves.[37] While it seems that SAW is more versatile and bio-compatible than other active methods for fission, the cost and complexity of operational instruments make it worthwhile to search for an alternative active method for droplet splitting.

Microvalves fabricated in deformable, multilayer, PDMS structures have been used to control on-chip fluid flows since their conception.[60] These pneumatic valves offer simplicity, ease of fabrication, high-power density, bio-compatibility and versatility,[61,62] and multiple valves can be controlled independently and simultaneously.[63] Their ability to control fluid behaviour has also meant they have been applied to two phase systems; generating[64,65], sorting[66], merging[65] and mixing[67,68] has been achieved. In most cases, the deformation of the channel geometry caused by valve operation causes a number of droplets to demonstrate altered behaviour, whether that is droplet size upon generation or toggling between merging and non-merging events. This is also the case for a previous study on valve usage for control of droplet splitting,[64] in which the size of batches of daughter droplets was controlled. Here, we apply the use of valves to pipetting from single droplets, studying the ability to affect the behaviour of the first droplet to arrive at a junction after its geometry has been altered by the actuation of a valve.

For this purpose we use a single layer valve design,[69,70] this design incorporates the control and flow channels on one layer of PDMS, separated by a thin, and therefore deformable, membrane. Such a design has been previously used for droplet sorting, [71-73] here we will use it to change the geometry at the site of the entrance to a bypass channel. This bypass channel, is joined at both ends to the main channel, the concept is that, as a mother droplet passes down the main channel, a small portion of any

selected droplet can be broken off into the bypass channel, where there is the potential for merging and reaction onset. As such by having multiple bypass channels in a system, multiple simultaneous and controllable reactions can be observed. The prerequisite for this, which we address here, is the subdivision of a single selected droplet.

2 Methodology

2.1 Experimental set-up

The microchannels were formed in polydimethylsiloxane (PDMS), using a master mold fabricated by standard lithography and dry etching techniques. To characterizing the valve, PDMS channels with different stiffnesses were prepared by changing the mix ratio. The usual ratio of PDMS is 10 parts (by weight) Dow Corning Sylgard 184 Silicone Elastomer base mixed with 1 part (by weight) Dow Corning Sylgard 184 Silicone Elastomer Curing Agent, however, to form more flexible structures 20:1 and 25:1 were also used, the latter being the limit in terms of room condition curing. After curing, the PDMS was peeled off the silicon mold, access holes for inlets and outlet were punched, and then it was exposed to an air plasma for 18 seconds. It was bonded to a clean glass slide because its surface was activated.

The microchannel network as shown in Fig. 1(a), consists of components for droplet generation and droplet splitting section. It is envisaged that for future usage of the splitting technology we have developed, each droplet will be of a different chemical, produced by moving a nozzle between samples off chip,[16] or by individual droplet formation.[8] However, for this system, designed to test the capability of the splitting technology, a standard droplet generation approach was taken, and this consists of a T-junction, fed by oil and water. The width of both the continuous and dispersed inlet channels is 100 μm with a height of 133.8 μm, the result is monodisperse, high throughput droplet generation.[12,27] Once the droplets are formed on the chip, the next feature is the bypass channel at which we seek to demonstrate selective droplet subdivision. This division part consists of the main channel bifurcating at a standard T-junction, where the width of the secondary channel is half that of the main channel. This asymmetry in channel dimensions makes it possible to have different regimes of splitting without the actuation of the valve which is located at this junction. The benefit of this arrangement is that operating conditions can be found at which the system is at a knife edge between a splitting and non-splitting condition, the valve can then be activated selectively in order to tip the balance in favour of a splitting event occurring. The thinner branched channel subsequently rejoins the main channel, hence we term it a bypass loop. In future, we envisage that reactions of daughter droplets split from mother droplets containing different chemicals will take place within this bypass loop by use of standard merging techniques.[23,24]

Double[60,64-68] and single[69-73] layer valve design have been described in the literature. Here, we do not need to fully seal the valve, rather just alter the channel geometry, hence a single layer valve is ideal. In this type of valve, a membrane, consisting of a thin layer of soft PDMS, is located in a vertical plane between the main channel and a valve actuation chamber. Once pressurised, the valve actuation chamber causes the membrane to deform into the main channel, hence changing the channels physical geometry. Based on shapes of the deformation that extracted from previous studies on single-layer valves[74,75], we hypothesised that if the head of single layer valve is curved, more actuation would be observed especially in the splitting zone. After running and analysing a series of experiments, a mushroom-shaped valve (with 1000 μm length of the head) with membrane thickness 30 μm was selected with a PDMS mix ratio of 20:1.

The inlets and outlet of the microfluidic network were connected to a microfluidic flow control system (MFCS™-EZ, Fluigent system) by using polytetrafluoroethylene (PTFE) tubing. Further tubing connected the inlet of the valve control channel to a second Fluigent system to control the air pressure in the microvalve. Two different Fluigent systems were used in the main and control channels to avoid fluctuation in pressures. A synthetic oil (3M™ Novec™) was used as a continuous phase in which 2% surfactant (Pico-Surf™ 1, Sphere Fluidics, UK) was added, while Milli-Q water was used as a dispersed phase. A camera (Pixelink PL-B782U, Ottawa, Canada) was mounted on an inverted microscope (Olympus CKX53, Tokyo, Japan) to record videos and images from the chip.

The recorded images and videos were analysed using a custom code written in MATLAB® by the authors. Two successive frames of the videos were used to track the movement of the interface between the continuous and dispersed phases in *x* direction (with reference to Fig. 1(a)) to calculate the mother droplet velocity. The volumes of the mother and daughter droplets were also measured by pixel counting and multiplying the resulting area by the height of channel (133.8 μm). The deformation of the channel wall due valve actuation was measured by edge location.

2.2 Numerical methods

To probe the flow physics of the system, a numerical model was utilized. The simulation used a finite volume method with the PISO (Pressure-implicit with splitting of operators) in ANSYS Fluent® v15 to numerically solve the 3D Navier-Stokes equation. In addition, a VOF (Volume-of-Fluid) method was used to trace the liquid-liquid interface and examine the droplet behaviour at the entrance of the microfluidic bypass loop. A mother droplet with the same volume and velocity as those in experiments was placed, initially, upstream of the inlet to the bypass loop. The outlet was set to atmospheric pressure while a no slip boundary condition was imposed on all walls. The continuous phase density and dynamic viscosity were set at 1614 kg m^{-3} and 0.77 mPa s, respectively, while for the dispersed phase these values were selected as at 998.2 kg m^{-3} and 1.003 mPa s, respectively. A contact angle of 135^0 between the two phases at the PDMS wall was extracted from the experimental video frames and used in the simulation. The surface tension between the continuous and dispersed phases was set to 18.5 mN/m. To numerically simulate the splitting mechanism at the valve, the dimensions of the deformed valves was measured experimentally and imposed in the model as a bulge in the channel wall.

3 Working Principle

The microfluidic chip design as can be seen in Fig. 1(a) consists of the main and secondary channels. The hydrodynamic resistance and the pressure drop of a rectangular channel can be calculated by the equations below[76],

$$R = \frac{12\mu L}{\omega h^3 \left[1 - 0.63\left(h/\omega\right)\right]} \quad (1)$$

$$\Delta P = RQ \quad (2)$$

where, ω, h and L denote width, height and length of the rectangular channel, respectively. In addition, Q, R and ΔP represent flow rate, resistance and pressure drop. So, in our design, the narrower and longer secondary channel (subscript S) has higher resistance and lower flow rate rather than the main channel (subscript M) due to the equality in differences between the pressure of the inlet (P_i) and pressure of the outlet (P_0) of the loop.

$$P_0 - P_i = \Delta P_M = \Delta P_S \quad (3)$$

Based on the fact that for a series resistance network, the total resistance equals the sum of the individual resistances and by applying Eq. (2) into Eq. (3):

$$(R_D + R_M)Q_M = R_S Q_S \quad (4)$$

where the subscript D denotes the resistance past the deformable valve. In addition, mass conservation of the fluid gives:

$$Q_T = Q_M + Q_S \quad (5)$$

where Q_T denotes the total flow.

By applying Eq. (4) into Eq. (5), Eq. (6) derives as:

$$Q_S = Q_T[1 + (R_S/(R_D + R_M))]^{-1} \quad (6)$$

In the absence of the droplet and before valve actuation, the pressure balance between the main and the high resistance secondary channel ensures that most of the flow passes through the main channel. Based on Eq. (1), actuating the valve decreases the width of the entrance of the loop and so increases the

hydrodynamic resistance of the deformable part of the main channel, R_D. This causes more fluid to pass via the secondary channel.

When two different phases (continuous and dispersed phases) are present in the microfluidic channel, additional pressure changes occur over the interfaces between two phases due to the surface tension.[77]

$$\Delta P = RQ + 2\gamma H \tag{7}$$

where, γ and H are the interfacial tension between the two phases and mean curvature of the interface, respectively. The mean curvature of interface is the inverse of radius of curvature based on Young-Laplace equation. [77,78]

By substituting Eq. (7) in Eq. (3), Eq. (8) derives as:

$$(R_D + R_M)Q_M + 2\gamma H_M = R_S Q_S + 2\gamma H_S \tag{8}$$

Here, $H_M=1/r_M$ and $H_S=1/r_S$. Finally, replacing Eq. (8) in Eq. (5) results in:

$$Q_S = (Q_T - [2\gamma(H_S - H_M)])[1 + (R_S/(R_D + R_M))]^{-1} \tag{9}$$

Hence, in the presence of droplets, upon actuation of the valve two effects promote a higher flow rate in the bypass channel. These are the change in flow resistance and the change in the curvature of the front of the droplet. In the latter, as the droplet passes the constriction the curvature of the front interface in the main channel, H_M is increased (Fig. 1 (b)). Our numerical analysis confirms this. We placed a constriction, similar in size to the operating valve, opposite the entrance to the bypass channel in one model, and opposite its exit in a second model. In the latter, only the flow resistance change will be relevant to the finger length created in the entrance of the bypass channel. Whilst in the former the radius change of the front interface will also play a role. When we plotted the finger length as a function of time, we saw an increase of 30% in the finger length when the constriction was at the entrance to the bypass confirming the additional effect of the deformed interface of the droplet.

Under certain flow conditions, when there is no valve actuation, we can expect the droplet to pass along the main channel intact, a finger into the bypass channel will develop, but it will then retract and the droplet will not split. However, when the valve is actuated, we can expect the two effects identified here to increase the flow into the bypass channel, and hence increase the finger length. This gives the possibility of using the valve to move from a non-break up condition (Fig. 1 (a)) to a break-up condition (Fig. 1 (c)) for the droplet.

4 Results & discussion

We first explore the operating conditions when the valve is not activated, showing that depending on the inlet pressure of the oil and water phases, the droplets formed may or may not split at the entrance to the bypass channel. In Fig. 2(a) the two inlet pressures were varied independently between 0 and 900 mbar, four regimes were observed in the splitting behaviour. *Non-splitting regime* for the case that none of the droplets which passed through the inlet of the loop is split, a *transition regime* in which less than 10% of droplets are split, and *low efficiency splitting regime* (LESR) and *high efficiency splitting regime* (HESR) in which between 10% and 50% and more than 50% of droplets are split, respectively. An increase in water inlet pressure, whilst oil inlet pressure is constant, gives rise to larger mother droplets, as can be seen by comparing Figs. 2(b) i and ii. Whilst, at higher oil pressure, and a fixed water pressure, smaller droplet are formed, as shown in Figs. 2(b) ii and iii. If the ratio between the pressure in the dispersed and continuous phases is fixed, then the mother droplet size is fixed, this can be seen from Figs. 2(b) i and iii, and is also true for Figs. 2(b) ii & iv. It should be noted here that whilst the splitting outcome of i and iii is the same (splitting does not occur), this is not true for the latter, case ii does not split, whilst iv does. Clearly, splitting events are not dictated by droplet size alone. In case iv, daughter droplets are created each time a mother droplet passes the entrance to the bypass, as such multiple droplets are seen in the bypass channel, this gives an indication of the relatively slow speed of fluid motion in the bypass compared to the main channel.

To explore the effect of the valve, the same pressure ranges are tested for each inlet, however, the valve is also pressurised at 800 mbar. Again, splitting behaviour is characterised using the same four regime descriptions, the results are shown in Fig. 2(c). Here, the transition regime has shifted leftward (towards lower water pressures). What we observe from the experiments is that in each case, the finger length formed is significantly larger than that of the non-activated valve case. Comparison between Figs. 2(b) ii and vi shows that actuating the valve to 800mbar results in breaking up some of the droplet, whilst for the unactuated valve no splitting was observed. To relate this shift in behaviour to the valve actuation pressure, the data from further experiments with two additional valve pressures have been summarised by simply plotting a line following the transition region for each case in Fig 2(d). It can be seen that with increasing valve pressure, as the channel constricts further, the transient regime is shifted further towards low water pressures. When a valve pressure of 1100 mbar is used, the droplets are split in all cases. This initial data set clearly shows that we can control the breakup region by actuating the valve.

In Fig. 2, the regimes are classified by the frequency and size of mother droplets, we now explore the valve efficiency further. In Fig. 3(a), the valve efficiency is shown as a function of valve pressure for a range of different inlet pressure conditions (the inset shows the location of these conditions on the same axes used in Fig. 2(d)). The valve efficiency is defined as the ratio of the number of split droplets in the bypass channel to the total number of droplets that pass the inlet to this loop. In each case, it can be seen that, for a fixed set of inlet conditions, increasing the actuation pressure of the valve increases the efficiency up to 1000 mbar. Above this valve pressure, some of the daughter droplets, that are formed, re-enter the main channel. This seems to occur as the deformation is such that the main channel is narrower than the bypass channel.

Comparison between different lines in Fig. 3(a) shows that for the same continuous phase inlet condition (Oil Pressure = 500mbar), increasing the water pressure increased the valve efficiency, this is because larger mother droplets are formed at the droplet generation T-junction, as shown in the inset of Fig 3(a). When these larger mother droplets interact with the entrance to the bypass channel, longer fingers are formed in the entrance and so even in the absence of the valve, they are closer to the condition at which splitting occurs. Hence a small bulge in the valve is required to switch regime, such that splitting occurs. The opposite trend is observed if the oil pressure is increased, whilst the water pressure is kept constant (Water Pressure = 500mbar). It should be noted here that the efficiency never goes above 60% in the experiments conducted. In the context of splitting every droplet, this would be a poor outcome. However, in the application of selective delivery of individual daughter droplets, the key feature is the repeatability of the splitting of the first droplet. Conceptually, the droplet of interest would be identified, and the valve actuated, what is desirable is that this, and only this droplet is then split i.e. selective breakup of a droplet. Next we re-examine the notion of efficiency in this context.

Fig. 4 shows a series of images of the entrance to the bypass channel. In the absence of valve actuation, the pressure imposed in the inlets of continuous and dispersed phases can be fully controlled and brought near the transition line between non-splitting and splitting, the conditions used here are Oil Pressure = 400mbar and Water Pressure = 500mbar (Fig. 4 (a)).

Increasing the pressure of valve gradually, increases the maximum finger length until, at a specific valve pressure, here 600 mbar, droplets randomly start to break up (Fig. 4 (b)). In the case shown, the sixth droplet which passes after valve actuation was split. This breaking up happens during the retreating of the droplet to the main channel and can be considered as a retarded breakup.[78]

Again, this is not desirable when selectivity is of interest. However, if the valve pressure is further increased by between 50-100 mbar the result is that the first droplet is split. An example of this repeatable effect is shown in Fig. 4(c). Once the daughter droplet is in the bypass channel, subsequent droplets do not split, so the valve efficiency, as detailed in Fig 3, remains low, but the desired droplet is split. This occurs as the presence of the daughter droplet in the bypass channel causes a change in the pressure balances. This could be rectified by changing the design of the bypass channel, for example, if the droplets are well spaced, then the speed of valve deflation can be slower than the interspacing time between droplets. Fig. 5 demonstrates this effect over a wider range of conditions, here the valve pressure required to randomly split a droplet is compared to the slightly higher value required to ensure the first droplet during valve actuation is split. It can be seen that the increase required, in the valve

pressure, is no more than 100mBar. Images of droplet behaviour are is shown for different cases of valve pressure in Fig 5(b).

To confirm this, Fig. 6 shows the valve operating at 650 mbar for Oil Pressure = 400 mbar & Water Pressure = 500 mbar at different time instances. As it can be seen, exactly the first mother droplet which passed the loop during actuation of valve split, subsequently for the duration of time in which the daughter droplet is in the loop, no further mother droplet split. This shows that the valve can split only the targeted droplet, which is beneficial for selectivity, if the correct actuation pressure is selected. In addition, it can be seen that the time response of the valve is around 0.05s which makes it at least 20 times faster than an earlier SAW actuated selective droplet splitting system.[37]

To examine the size of the daughter droplet formed, Fig. 7(a) measures the length of the finger drawn into the bypass channel, it can be seen from the range of conditions examined that the length of the finger grows continuously with time as the mother droplets passes the bypass entrance. This occurs with or without valve actuation. Comparison between Figs. 7(a) i & ii shows that when valve is actuated with 1000 mbar pressure, the maximum finger size is approximately increased by 135% for these small mother droplets, while for larger mother droplets only 55% increment in size has been observed by comparison between Figs. 7(a) iii & v. The corresponding finger lengths are shown in Fig. 7(b).

As a result of this lesser effect on the finger length for the larger droplets, the range of daughter droplet sizes that can be produced are smaller. Fig. 8(a) shows the relative volume of daughter droplet to the mother droplet versus the valve pressure for two inlet conditions which produce different mother droplet volumes. The droplet breakup with different relative volumes obtained at different valve pressures, indicated in Fig. 8(a), and predicted by the numerical simulations shown in Fig. 8(b and c), are shown in Fig. 8(d). It can be seen in Fig. 8(a) that the range of relative volume of daughter droplets are up to approximately 10% for larger droplets and 20% for the smaller mother droplets. The maximum ratio is split from the main droplet when valve is working in the optimum pressure of 1000 mbar. This demonstrates that inlet pressures, which control mother droplet volume can be used to set the range of daughter droplet volumes which can be produced. For example, if a narrow range is required which shows little variation with valve pressure, and hence is robust to fluctuations, then longer droplets should be used. Whilst for the ability to dispense droplets of different sizes a shorter mother droplet is desirable.

5 Conclusions

As a novel, efficient and compact high throughput screening system, our system uses a single layer valve to split droplets on demand. A microfabricated membrane is pressurised to deform precisely which selectively breaks up desired droplets. Control over the pressure of two inlets and one valve simultaneously, gives users the ability to completely dictate the range of droplets that can be produced in the new splitting system. The effect of pressure induced in the valve on the daughter droplet sizes was also numerically investigated which qualitatively validated the trend observed experimentally and the results was used to back up the underlying physics of proposed system. Being cheap, simple, high speed and selective, are some of the advantages of our newly-introduced splitting system. Besides, when our splitting technique is combined with the traditional merging system, it can be used as a high throughput system for combinatorial library purposes. More studies for the evaluation of the effect of ejected daughter droplets on the pressure in the main and secondary channels needs to be done to show that successive bypass loops can be used as independent units for on demand splitting and merging.

Bibliography

(1) Brouzes, E.; Medkova, M.; Savenelli, N.; Marran, D.; Twardowski, M.; Hutchison, J. B.; Rothberg, J. M.; Link, D. R.; Perrimon, N.; Samuels, M. L. *Proceedings of the National Academy of Sciences* **2009**, *106*, 14195-14200.
(2) Shestopalov, I.; Tice, J. D.; Ismagilov, R. F. *Lab on a Chip* **2004**, *4*, 316-321.
(3) Hung, L.-H.; Choi, K. M.; Tseng, W.-Y.; Tan, Y.-C.; Shea, K. J.; Lee, A. P. *Lab on a Chip* **2006**, *6*, 174-178.

(4) Frenz, L.; El Harrak, A.; Pauly, M.; Bégin-Colin, S.; Griffiths, A. D.; Baret, J. C. *Angewandte Chemie International Edition* **2008**, *47*, 6817-6820.
(5) Bocanegra, R.; Luis Sampedro, J.; Gañán-Calvo, A.; Marquez, M. *Journal of microencapsulation* **2005**, *22*, 745-759.
(6) Li, J.; Barrow, D. *Lab on a Chip* **2017**, *17*, 2873-2881.
(7) Min, N. G.; Ku, M.; Yang, J.; Kim, S.-H. *Chemistry of Materials* **2016**, *28*, 1430-1438.
(8) Kang, D.-K.; Gong, X.; Cho, S.; Kim, J.-y.; Edel, J. B.; Chang, S.-I.; Choo, J.; deMello, A. J. *Analytical chemistry* **2015**, *87*, 10770-10778.
(9) Berg, M.; Undisz, K.; Thiericke, R.; Zimmermann, P.; Moore, T.; Posten, C. *Journal of biomolecular screening* **2001**, *6*, 47-56.
(10) Janzen, W. P. In *Molecular Biomethods Handbook*; Springer, 2008, pp 1097-1118.
(11) Sesen, M.; Alan, T.; Neild, A. *Lab on a Chip* **2017**, *17*, 2372-2394.
(12) Thorsen, T.; Roberts, R. W.; Arnold, F. H.; Quake, S. R. *Physical review letters* **2001**, *86*, 4163.
(13) Niu, X.; Gielen, F.; Edel, J. B. *Nature chemistry* **2011**, *3*, 437-442.
(14) Zec, H.; Rane, T. D.; Wang, T.-H. *Lab on a Chip* **2012**, *12*, 3055-3062.
(15) Theberge, A. B.; Mayot, E.; El Harrak, A.; Kleinschmidt, F.; Huck, W. T.; Griffiths, A. D. *Lab on a chip* **2012**, *12*, 1320-1326.
(16) Gielen, F.; van Vliet, L.; Koprowski, B. T.; Devenish, S. R.; Fischlechner, M.; Edel, J. B.; Niu, X.; deMello, A. J.; Hollfelder, F. *Analytical chemistry* **2013**, *85*, 4761-4769.
(17) Anna, S. L.; Bontoux, N.; Stone, H. A. *Applied physics letters* **2003**, *82*, 364-366.
(18) Dreyfus, R.; Tabeling, P.; Willaime, H. *Physical review letters* **2003**, *90*, 144505.
(19) Cramer, C.; Fischer, P.; Windhab, E. J. *Chemical Engineering Science* **2004**, *59*, 3045-3058.
(20) Sugiura, S.; Nakajima, M.; Tong, J.; Nabetani, H.; Seki, M. *Journal of colloid and interface science* **2000**, *227*, 95-103.
(21) Sugiura, S.; Nakajima, M.; Iwamoto, S.; Seki, M. *Langmuir* **2001**, *17*, 5562-5566.
(22) Tan, Y.-C.; Ho, Y. L.; Lee, A. P. *Microfluidics and Nanofluidics* **2007**, *3*, 495-499.
(23) Bremond, N.; Thiam, A. R.; Bibette, J. *Physical review letters* **2008**, *100*, 024501.
(24) Niu, X.; Gulati, S.; Edel, J. B. *Lab on a chip* **2008**, *8*, 1837-1841.
(25) Lee, S.; Kim, H.; Won, D.-J.; Lee, J.; Kim, J. *Microfluidics and Nanofluidics* **2016**, *20*, 1.
(26) Tullis, J.; Park, C. L.; Abbyad, P. *Lab on a Chip* **2014**, *14*, 3285-3289.
(27) Gu, H.; Duits, M. H.; Mugele, F. *International journal of molecular sciences* **2011**, *12*, 2572-2597.
(28) Feng, S.; Yi, L.; Zhao-Miao, L.; Ren-Tuo, C.; Gui-Ren, W. *Chinese Journal of Analytical Chemistry* **2015**, *43*, 1942-1954.
(29) Liu, K.; Ding, H.; Chen, Y.; Zhao, X.-Z. *Microfluidics and Nanofluidics* **2007**, *3*, 239-243.
(30) Yoon, D. H.; Jamshaid, A.; Ito, J.; Nakahara, A.; Tanaka, D.; Akitsu, T.; Sekiguchi, T.; Shoji, S. *Lab on a Chip* **2014**, *14*, 3050-3055.
(31) Eow, J. S.; Ghadiri, M. *Colloids and Surfaces A: Physicochemical and Engineering Aspects* **2003**, *219*, 253-279.
(32) Ahn, K.; Agresti, J.; Chong, H.; Marquez, M.; Weitz, D. *Applied Physics Letters* **2006**, *88*, 264105.
(33) Priest, C.; Herminghaus, S.; Seemann, R. *Applied Physics Letters* **2006**, *89*, 134101.
(34) Mousavichoubeh, M.; Ghadiri, M.; Shariaty-Niassar, M. *Chemical Engineering and Processing: Process Intensification* **2011**, *50*, 338-344.
(35) Sesen, M.; Alan, T.; Neild, A. *Lab on a Chip* **2014**, *14*, 3325-3333.
(36) Jin, S. H.; Jeong, H.-H.; Lee, B.; Lee, S. S.; Lee, C.-S. *Lab on a Chip* **2015**, *15*, 3677-3686.
(37) Sesen, M.; Devendran, C.; Malikides, S.; Alan, T.; Neild, A. *Lab on a Chip* **2017**, *17*, 438-447.
(38) Jung, J. H.; Destgeer, G.; Ha, B.; Park, J.; Sung, H. J. *Lab on a Chip* **2016**, *16*, 3235-3243.
(39) Adamson, D. N.; Mustafi, D.; Zhang, J. X.; Zheng, B.; Ismagilov, R. F. *Lab on a Chip* **2006**, *6*, 1178-1186.
(40) Teh, S.-Y.; Lin, R.; Hung, L.-H.; Lee, A. P. *Lab on a Chip* **2008**, *8*, 198-220.
(41) Hatch, A. C.; Fisher, J. S.; Tovar, A. R.; Hsieh, A. T.; Lin, R.; Pentoney, S. L.; Yang, D. L.; Lee, A. P. *Lab on a chip* **2011**, *11*, 3838-3845.
(42) De Menech, M. *Physical Review E* **2006**, *73*, 031505.
(43) Afkhami, S.; Leshansky, A.; Renardy, Y. *Physics of Fluids* **2011**, *23*, 022002.

(44) Tan, Y.-C.; Fisher, J. S.; Lee, A. I.; Cristini, V.; Lee, A. P. *Lab on a Chip* **2004**, *4*, 292-298.
(45) Yang, C.-G.; Xu, Z.-R.; Wang, J.-H. *TrAC Trends in Analytical Chemistry* **2010**, *29*, 141-157.
(46) Scheiff, F.; Mendorf, M.; Agar, D.; Reis, N.; Mackley, M. *Lab on a Chip* **2011**, *11*, 1022-1029.
(47) Seemann, R.; Brinkmann, M.; Pfohl, T.; Herminghaus, S. *Reports on progress in physics* **2011**, *75*, 016601.
(48) Link, D.; Anna, S. L.; Weitz, D.; Stone, H. *Physical review letters* **2004**, *92*, 054503.
(49) Clausell-Tormos, J.; Griffiths, A. D.; Merten, C. A. *Lab on a Chip* **2010**, *10*, 1302-1307.
(50) Um, E.; Rogers, M. E.; Stone, H. A. *Lab on a Chip* **2013**, *13*, 4674-4680.
(51) Link, D. R.; Grasland-Mongrain, E.; Duri, A.; Sarrazin, F.; Cheng, Z.; Cristobal, G.; Marquez, M.; Weitz, D. A. *Angewandte Chemie International Edition* **2006**, *45*, 2556-2560.
(52) de Ruiter, R.; Pit, A. M.; de Oliveira, V. M.; Duits, M. H.; van den Ende, D.; Mugele, F. *Lab on a Chip* **2014**, *14*, 883-891.
(53) Baroud, C. N.; de Saint Vincent, M. R.; Delville, J.-P. *Lab on a Chip* **2007**, *7*, 1029-1033.
(54) Baroud, C. N.; Delville, J.-P.; Gallaire, F.; Wunenburger, R. *Physical Review E* **2007**, *75*, 046302.
(55) Ting, T. H.; Yap, Y. F.; Nguyen, N.-T.; Wong, T. N.; Chai, J. C. K.; Yobas, L. *Applied Physics Letters* **2006**, *89*, 234101.
(56) Yap, Y.-F.; Tan, S.-H.; Nguyen, N.-T.; Murshed, S. S.; Wong, T.-N.; Yobas, L. *Journal of Physics D: Applied Physics* **2009**, *42*, 065503.
(57) Cho, S. K.; Moon, H.; Kim, C.-J. *Journal of microelectromechanical systems* **2003**, *12*, 70-80.
(58) Geng, H.; Feng, J.; Stabryla, L. M.; Cho, S. K. In *2017 IEEE 30th International Conference on Micro Electro Mechanical Systems (MEMS)*, 2017, pp 113-116.
(59) Sesen, M.; Alan, T.; Neild, A. *Lab on a Chip* **2015**, *15*, 3030-3038.
(60) Unger, M. A.; Chou, H.-P.; Thorsen, T.; Scherer, A.; Quake, S. R. *Science* **2000**, *288*, 113-116.
(61) De Volder, M.; Reynaerts, D. *Journal of Micromechanics and microengineering* **2010**, *20*, 043001.
(62) Au, A. K.; Lai, H.; Utela, B. R.; Folch, A. *Micromachines* **2011**, *2*, 179-220.
(63) Yetisen, A. K.; Coskun, A. F.; England, G.; Cho, S.; Butt, H.; Hurwitz, J.; Kolle, M.; Khademhosseini, A.; Hart, A. J.; Folch, A. *Advanced Materials* **2016**, *28*, 1724-1742.
(64) Choi, J.-H.; Lee, S.-K.; Lim, J.-M.; Yang, S.-M.; Yi, G.-R. *Lab on a Chip* **2010**, *10*, 456-461.
(65) Zeng, S.; Li, B.; Su, X. o.; Qin, J.; Lin, B. *Lab on a Chip* **2009**, *9*, 1340-1343.
(66) Chen, Y.; Tian, Y.; Xu, Z.; Wang, X.; Yu, S.; Dong, L. *Applied Physics Letters* **2016**, *109*, 143510.
(67) Streets, A. M.; Zhang, X.; Cao, C.; Pang, Y.; Wu, X.; Xiong, L.; Yang, L.; Fu, Y.; Zhao, L.; Tang, F. *Proceedings of the National Academy of Sciences* **2014**, *111*, 7048-7053.
(68) Liu, J.; Williams, B. A.; Gwirtz, R. M.; Wold, B. J.; Quake, S. *Angewandte Chemie* **2006**, *118*, 3700-3705.
(69) Sundararajan, N.; Kim, D.; Berlin, A. A. *Lab on a Chip* **2005**, *5*, 350-354.
(70) Lee, S.; Chan, J. C.; Maung, K.; Rezler, E.; Sundararajan, N. *Journal of Micromechanics and Microengineering* **2007**, *17*, 843.
(71) Abate, A.; Weitz, D. *Applied Physics Letters* **2008**, *92*, 243509.
(72) Abate, A. R.; Romanowsky, M. B.; Agresti, J. J.; Weitz, D. A. *Applied Physics Letters* **2009**, *94*, 023503.
(73) Abate, A. R.; Agresti, J. J.; Weitz, D. A. *Applied Physics Letters* **2010**, *96*, 203509.
(74) Xi, H.-D.; Zheng, H.; Guo, W.; Gañán-Calvo, A. M.; Ai, Y.; Tsao, C.-W.; Zhou, J.; Li, W.; Huang, Y.; Nguyen, N.-T. *Lab on a Chip* **2017**, *17*, 751-771.
(75) Jamshaid, A.; Igaki, M.; Yoon, D. H.; Sekiguchi, T.; Shoji, S. *Micromachines* **2013**, *4*, 34-48.
(76) Bruus, H. *Theoretical microfluidics*; Oxford university press Oxford, 2007.
(77) Kirshner, J. M. *Design theory of fluidic components*; Academic Press, 2012.
(78) Ménétrier-Deremble, L.; Tabeling, P. *Physical Review E* **2006**, *74*, 035303.

Figure Captions

Figure 1: Depiction of the selective droplet partitioning system. (a) Mother droplets are produced in a T-junction and passes the entrance of the bypass loop when the valve is off. Non-splitting regime dominates under these conditions. (b) The valve is actuated which results in deforming the channel wall and guiding more fluid into the secondary channel. The finger length increases as a result of changing in flow resistance and curvature of the front of the droplet. (c) Under these conditions the mother droplet passes along the main channel after splitting has occured.

Figure 2: Classification of splitting regimes by the frequency and size of mother droplets (a) Regime map shows four splitting regimes in the absence of valve on Oil Pressure-Water Pressure plane; (1) Non-splitting Regime with black square markers (2) Transition Regime with red circle markers (3) LESR (Low efficiency splitting regime) with blue triangle markers (4) HESR (High efficiency splitting regime) with green diamond markers (b) Images showing droplet behaviour in the entrance of bypass loop in the absence (i) - (iv) and presence of 800 mbar activated valve (v) - (viii). (c) Regime map shows four splitting regimes in the presence of activated valve on the pressure of 800 mbar on Oil Pressure-Water Pressure plane. (d) Transient lines follow the transition regions showing the transition from non-splitting to splitting regimes in four different valve pressures; 0 mbar, 800 mbar, 1000 mbar and 1100 mbar.

Figure 3: The effect of valve pressure on the valve efficiency which is defined as the ratio of the number of split droplets in the bypass channel to the total number of droplets that pass the inlet of bypass loop (a) Four different pairs of oil and water pressures are studied here which is shown in the inset (b) Experimental images showing (i) - (v) valve has different efficiencies at different valve pressures for the fixed inlet condition of Oil Pressure = 400 mbar & Water Pressure = 500 mbar.

Figure 4: Timelapse images of droplet passing the entrance of bypass loop with the constant inlet conditions of Oil Pressure = 400 mbar & Water Pressure = 500 mbar (a) In the absence of actuated valve (b) After the valve is actuated to the pressure of 600 mbar. (c) During the valve actuation when 650 mbar is imposed in the valve inlet.

Figure 5: (a) Comparison between the pressure which is required to split droplets randomly and the pressure which is needed to split the first coming droplets for different inlet conditions (b) Experimental images for the indicated data points (i) - (v).

Figure 6: Timelapse images of the droplet passing through the entrance of the bypass loop in the operating condition of Oil Pressure = 400 mbar, Water Pressure = 500 mbar & valve pressure = 650 mbar which shows that the system is selective and on demand with the minimum possible actuation in the valve part.

Figure 7: (a) Plot shows the finger length as the function of frame numbers for small droplets (Oil Pressure = 800 mbar & Water Pressure = 500 mbar) and large droplets (Oil Pressure = 400 mbar & Water Pressure = 500 mbar) in the absence and presence of the valve that is actuated to 1000 mbar. (b) While in the absence of valve, finger reaches the maximum size of 74 μm (i) as valve is actuated finger reaches the maximum size of 174 μm (ii) for small droplets. On the other hand, for large droplets maximum finger lengths are 124 μm (iv) and 192 μm (v) in the absence and presence of actuated valve with the pressure of 1000 mbar.

Figure 8: (a) Plot shows the relative volume of daughter droplet to the mother droplet for small droplets (Oil Pressure = 800 mbar & Water Pressure = 500 mbar) and large droplets (Oil Pressure = 400 mbar & Water Pressure = 500 mbar). (b) Contours are extracted images from numerical simulation for the Deformation = 36 μm related to the Valve Pressure = 600 mbar, (1) before and (2) after of droplet passing the entrance of bypass loop. (c) Two images from numerical simulation are shown, (1) before and (2) after splitting of the mother droplet, this occurs for a Deformation of 40 μm equivalent to an

experimental Valve Pressure of 650 mbar, Results show that 7% and 8% of mother droplet split numerically and experimentally. (d) Experimental images for the indicated data points (i) - (vi).

Figures:

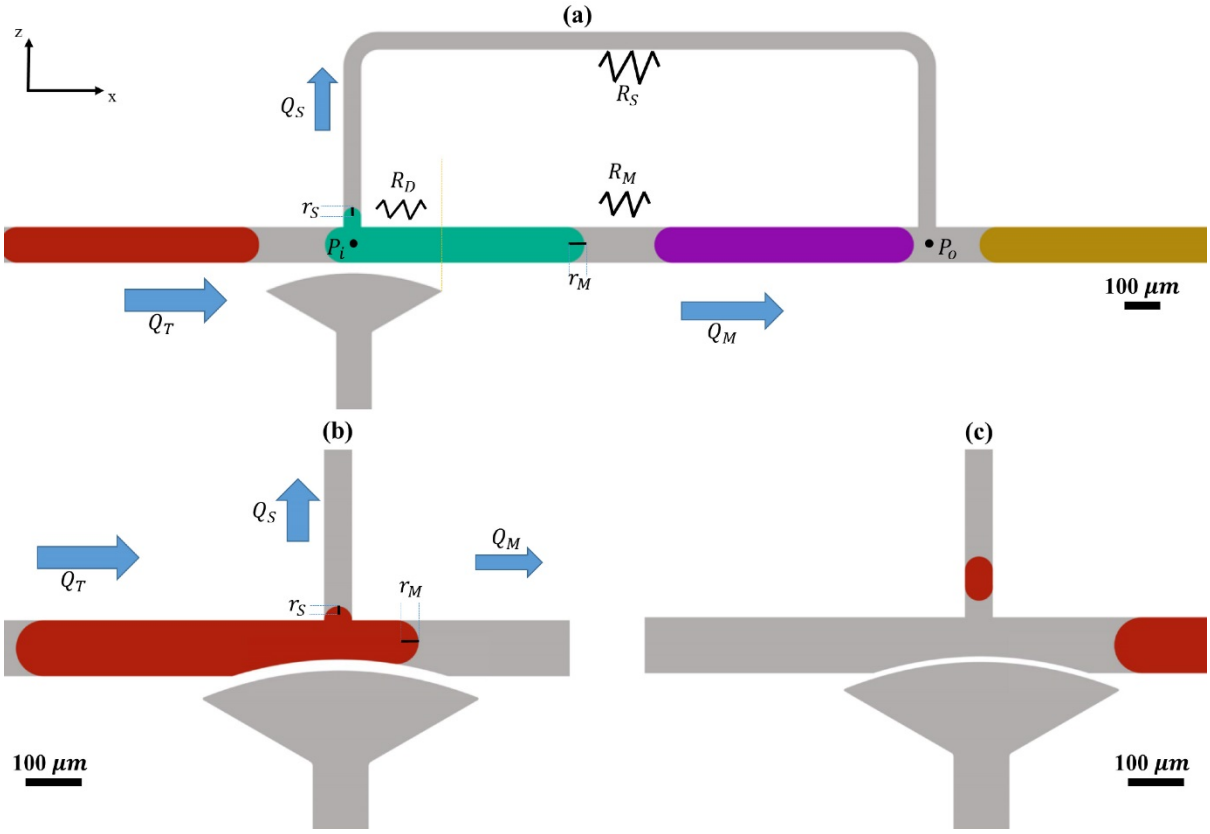

Fig. 1 Depiction of the selective droplet partitioning system. (a) Mother droplets are produced in a T-junction and passes the entrance of the bypass loop when the valve is off. Non-splitting regime dominates under these conditions. (b) The valve is actuated which results in deforming the channel wall and guiding more fluid into the secondary channel. The finger length increases as a result of changing in flow resistance and curvature of the front of the droplet. (c) Under these conditions the mother droplet passes along the main channel after splitting has occured.

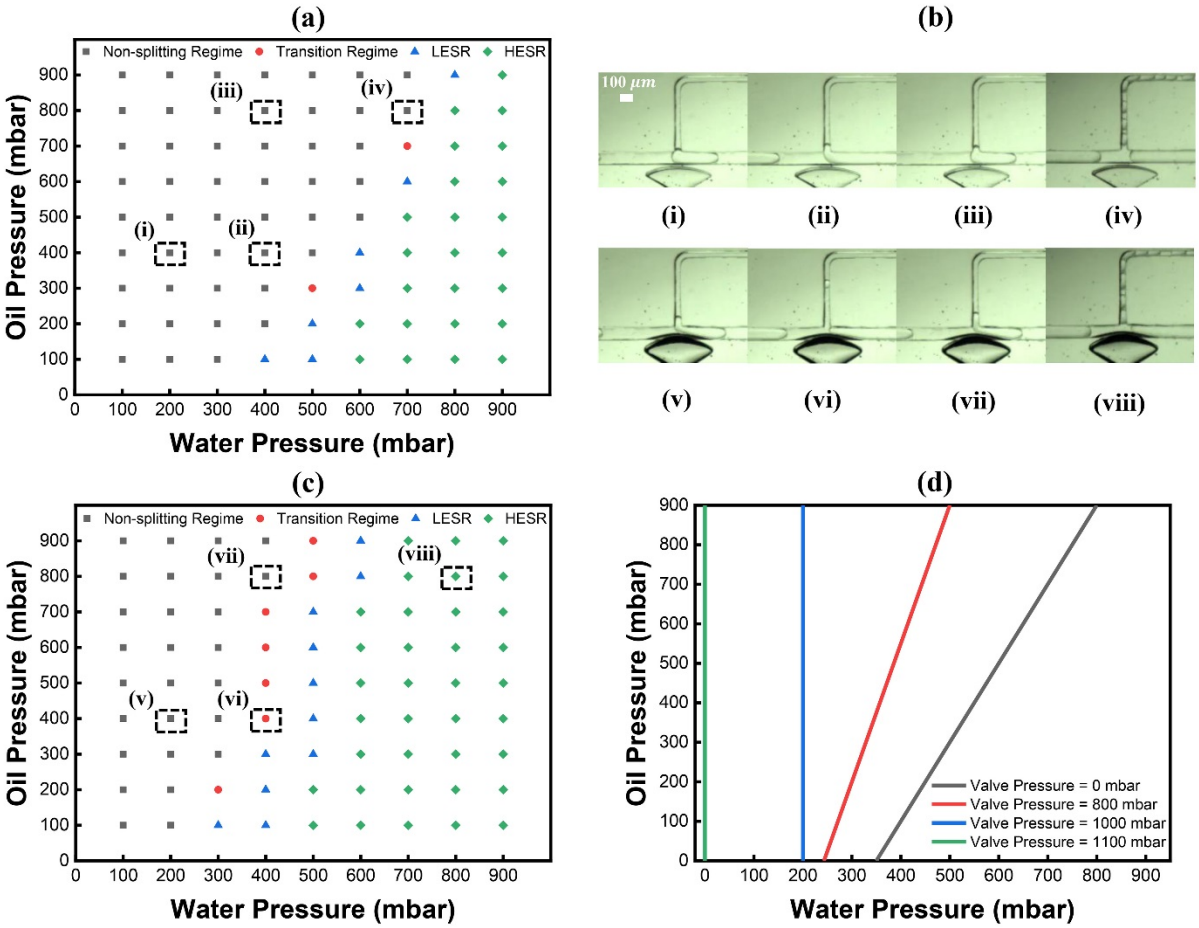

Fig. 2 Classification of splitting regimes by the frequency and size of mother droplets (a) Regime map shows four splitting regimes in the absence of valve on Oil Pressure-Water Pressure plane; (1) Non-splitting Regime with black square markers (2) Transition Regime with red circle markers (3) LESR (Low efficiency splitting regime) with blue triangle markers (4) HESR (High efficiency splitting regime) with green diamond markers (b) Images showing droplet behaviour in the entrance of bypass loop in the absence (i) - (iv) and presence of 800 mbar activated valve (v) - (viii). (c) Regime map shows four splitting regimes in the presence of activated valve on the pressure of 800 mbar on Oil Pressure-Water Pressure plane. (d) Transient lines follow the transition regions showing the transition from non-splitting to splitting regimes in four different valve pressures; 0 mbar, 800 mbar, 1000 mbar and 1100 mbar.

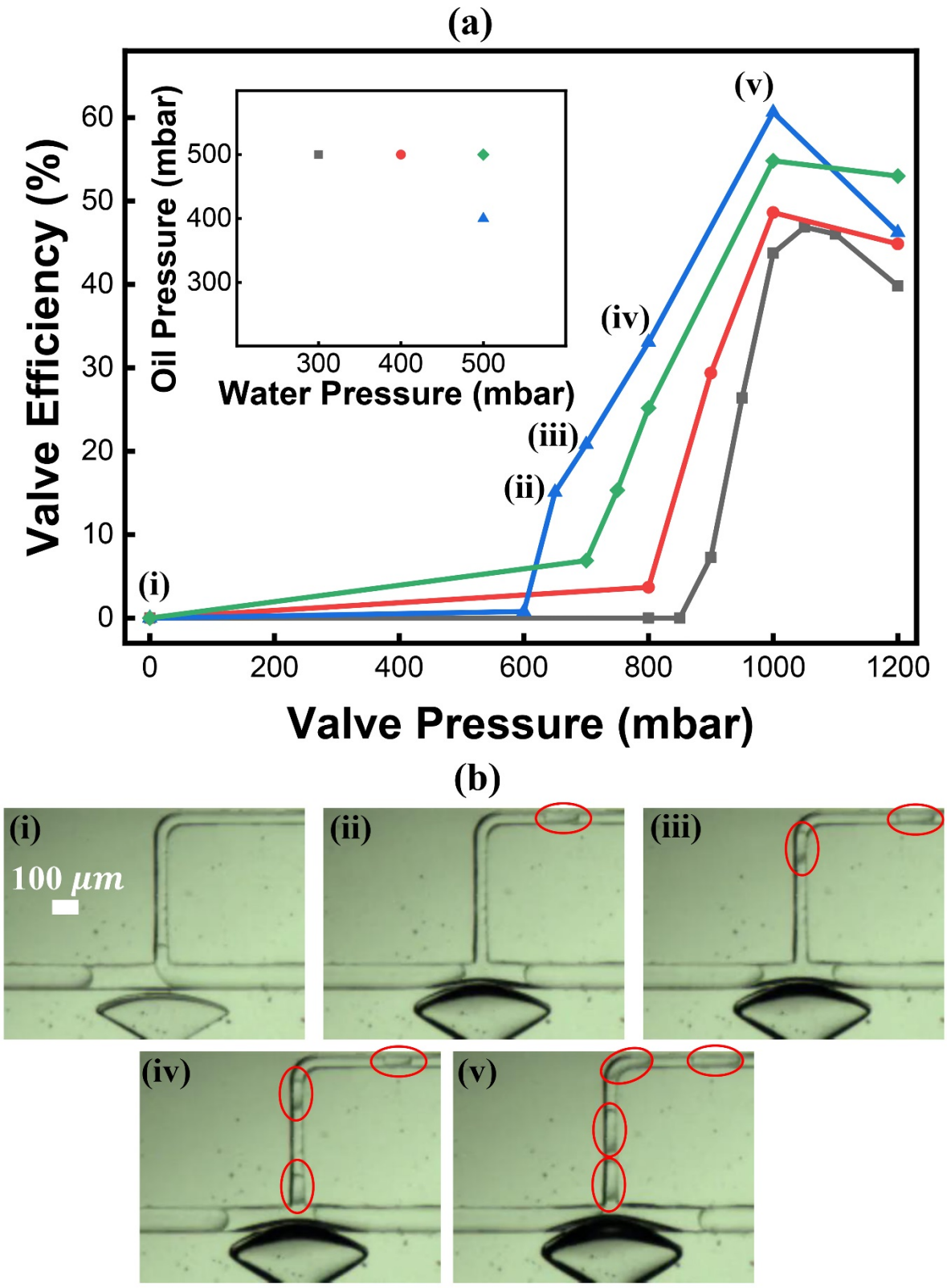

Fig. 3 The effect of valve pressure on the valve efficiency which is defined as the ratio of the number of split droplets in the bypass channel to the total number of droplets that pass the inlet of bypass loop (a) Four different pairs of oil and water pressures are studied here which is shown in the inset (b) Experimental images showing (i) - (v) valve has different efficiencies at different valve pressures for the fixed inlet condition of Oil Pressure = 400 mbar & Water Pressure = 500 mbar.

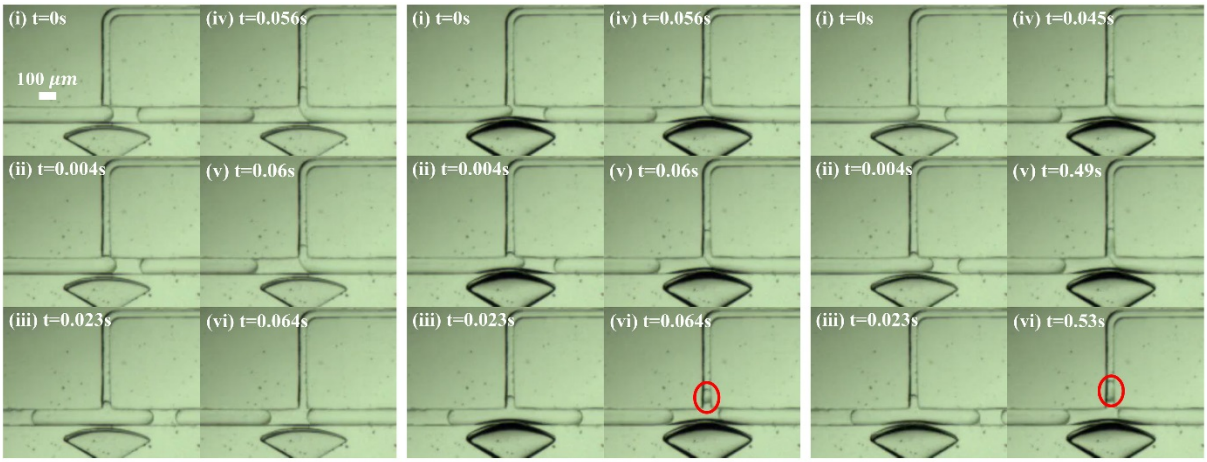

(a) Valve Pressure = 0 mbar **(b) Valve Pressure = 600 mbar** **(c) Valve Pressure = 650 mbar**

Fig. 4 Timelapse images of droplet passing the entrance of bypass loop with the constant inlet conditions of Oil Pressure = 400 mbar & Water Pressure = 500 mbar (a) In the absence of actuated valve (b) After the valve is actuated to the pressure of 600 mbar. (c) During the valve actuation when 650 mbar is imposed in the valve inlet.

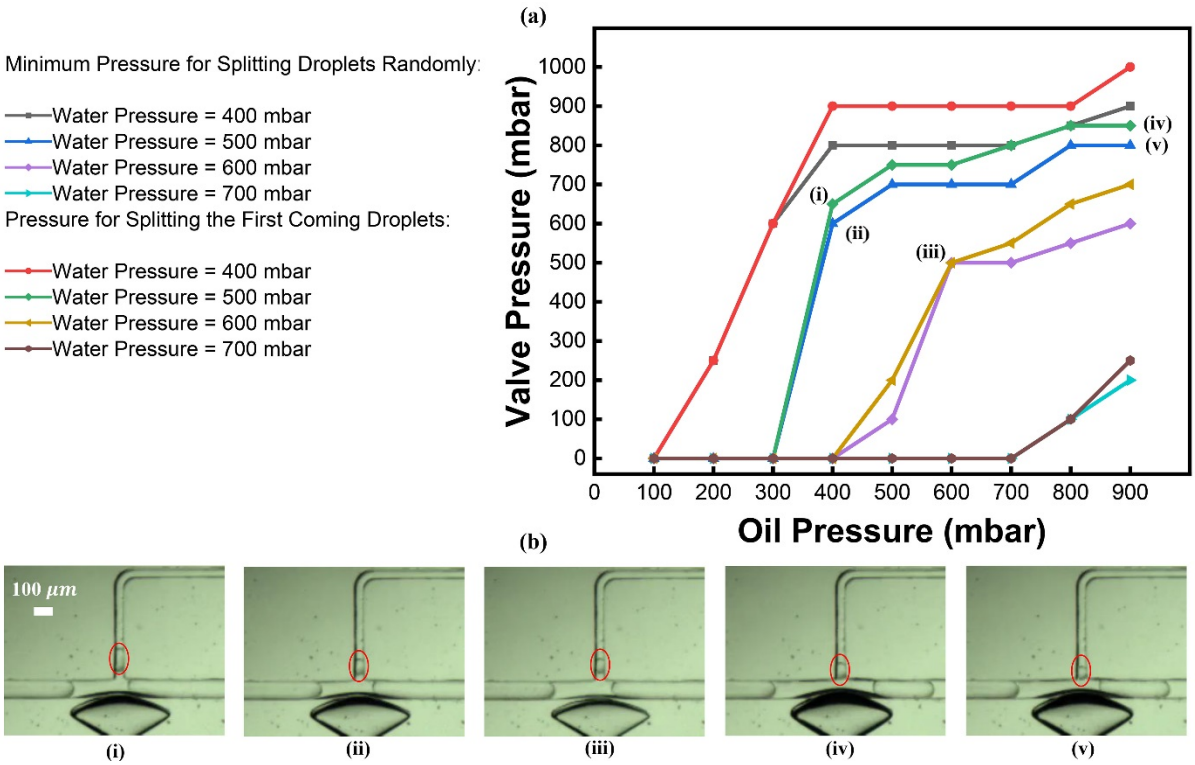

Fig. 5 (a) Comparison between the pressure which is required to split droplets randomly and the pressure which is needed to split the first coming droplets for different inlet conditions (b) Experimental images for the indicated data points (i) - (v).

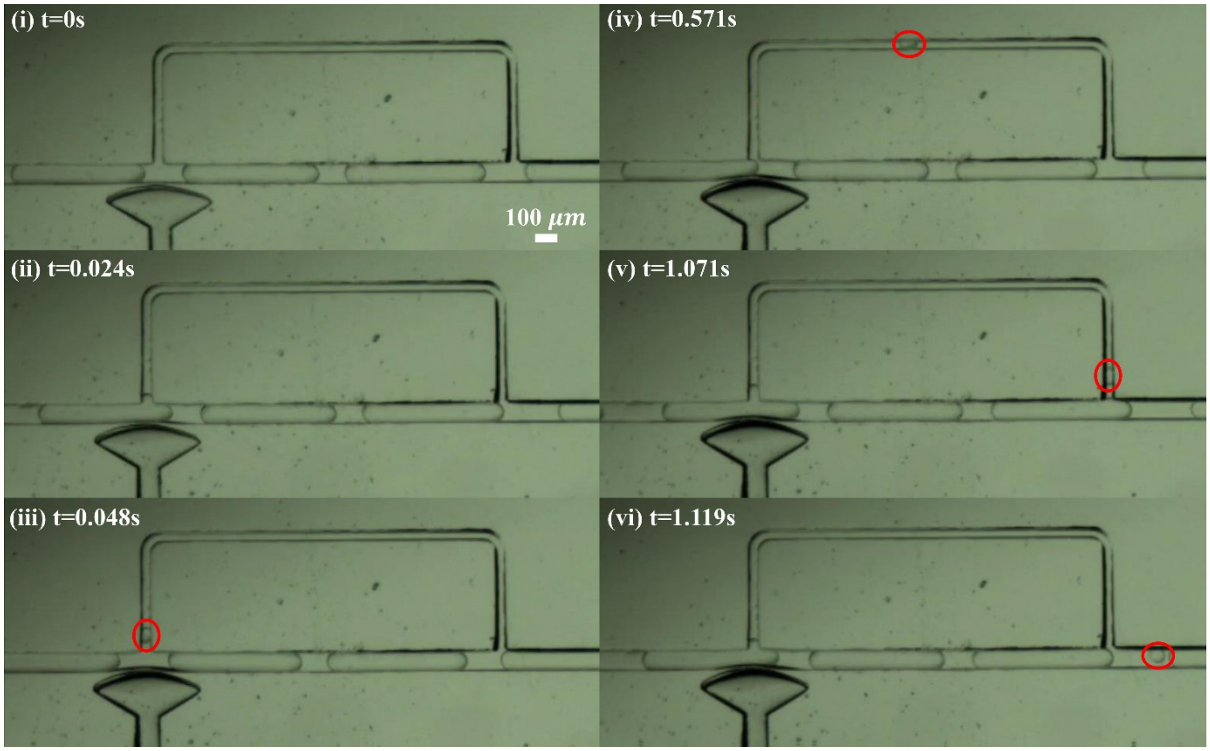

Fig. 6 Timelapse images of the droplet passing through the entrance of the bypass loop in the operating condition of Oil Pressure = 400 mbar, Water Pressure = 500 mbar & valve pressure = 650 mbar which shows that the system is selective and on demand with the minimum possible actuation in the valve part.

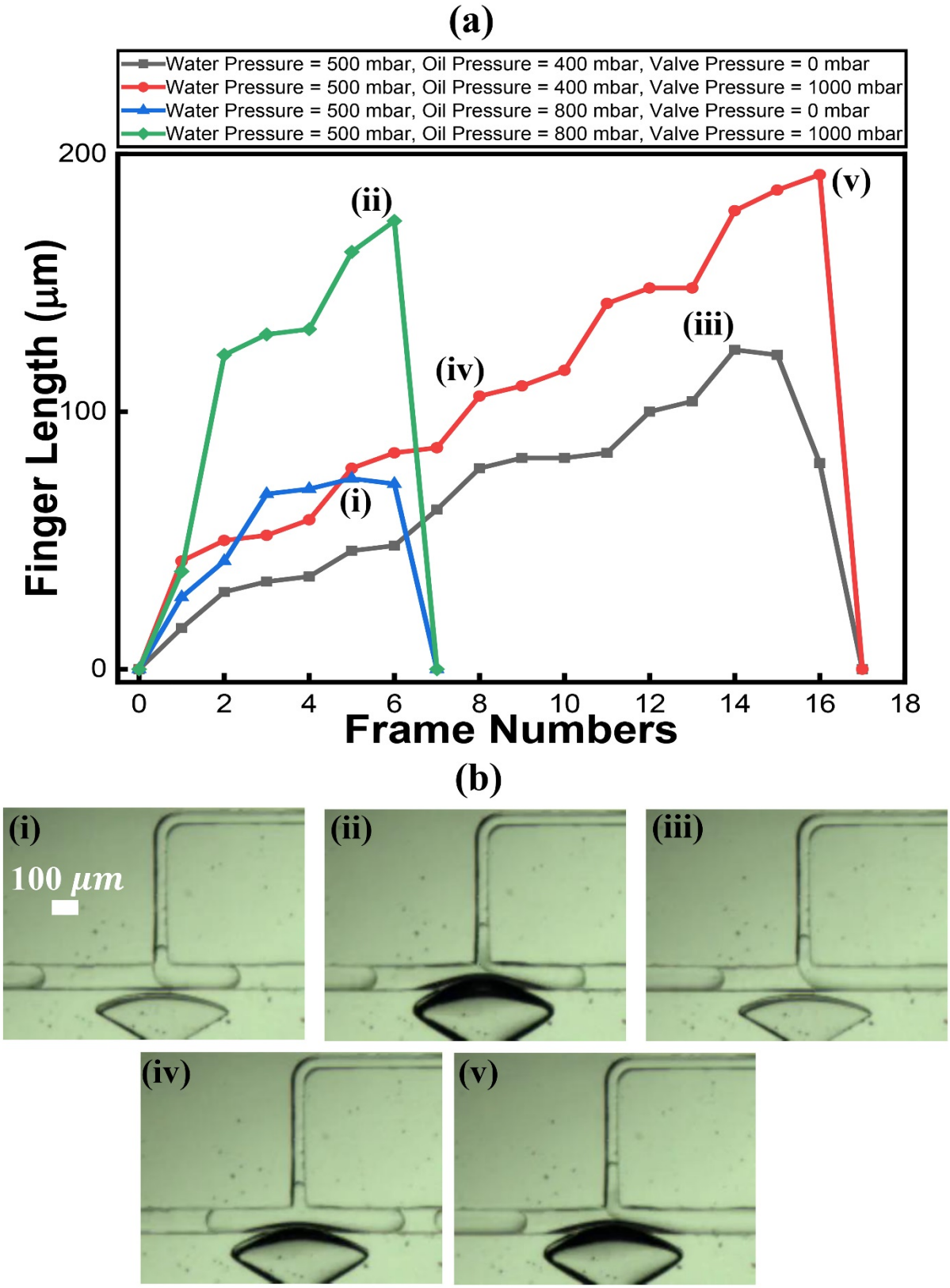

Fig. 7 (a) Plot shows the finger length as the function of frame numbers for small droplets (Oil Pressure = 800 mbar & Water Pressure = 500 mbar) and large droplets (Oil Pressure = 400 mbar & Water Pressure = 500 mbar) in the absence and presence of the valve that is actuated to 1000 mbar. (b) While in the absence of valve, finger reaches the maximum size of 74 μm (i) as valve is actuated finger reaches the maximum size of 174 μm (ii) for small droplets. On the other hand, for large droplets maximum finger lengths are 124 μm (iv) and 192 μm (v) in the absence and presence of actuated valve with the pressure of 1000 mbar.

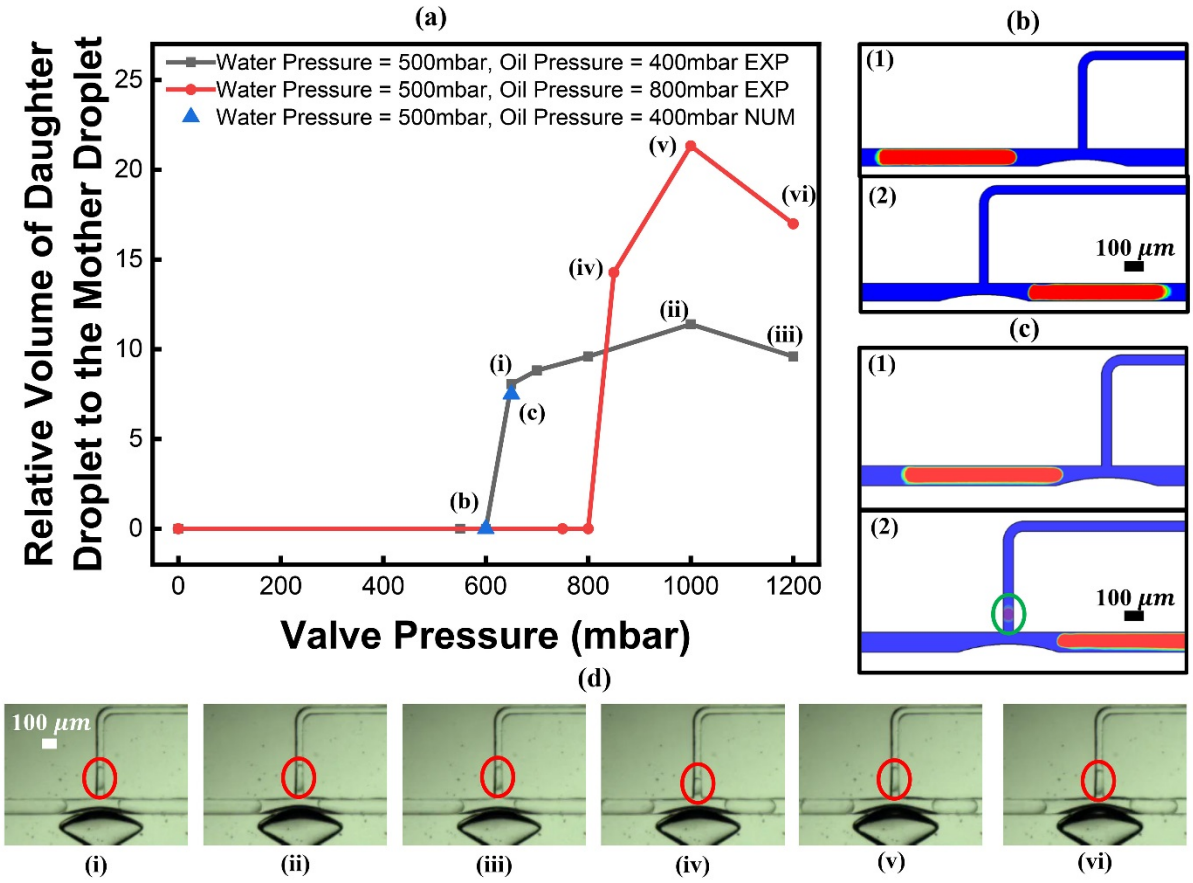

Fig. 8 (a) Plot shows the relative volume of daughter droplet to the mother droplet for small droplets (Oil Pressure = 800 mbar & Water Pressure = 500 mbar) and large droplets (Oil Pressure = 400 mbar & Water Pressure = 500 mbar). (b) Contours are extracted images from numerical simulation for the Deformation = 36 μm related to the Valve Pressure = 600 mbar, (1) before and (2) after of droplet passing the entrance of bypass loop. (c) Two images from numerical simulation are shown, (1) before and (2) after splitting of the mother droplet, this occurs for a Deformation of 40 μm equivalent to an experimental Valve Pressure of 650 mbar, Results show that 7% and 8% of mother droplet split numerically and experimentally. (d) Experimental images for the indicated data points (i) - (vi).